RSC Advances

ROYAL SOCIETY OF CHEMISTRY

www.rsc.org/advances

Journal Name

ARTICLE

Polymorphic phase study on Nitrogen-doped TiO_2 nanoparticles: Effect on oxygen site occupancy, dye sensitized solar cells efficiency and hydrogen production

Received 00th January 20xx,
Accepted 00th January 20xx

DOI: 10.1039/x0xx00000x

www.rsc.org/

Emerson C. Kohlrausch,[a] Maximiliano J. M. Zapata,[b] Renato V. Gonçalves,[c] Sherdil Khan,[b] Mauricio de O. Vaz,[b] Jairton Dupont,[d] Sérgio R. Teixeira,[b] Marcos J. L. Santos[a*]

In this work we show that phase formation and oxygen substitution can be controlled by the source of nitrogen used during the synthesis of TiO_2 nanoparticles. By perfoming a throught study on the structure of the nanoparticles, the use of NH_4^+ or NO_3^- was found to influence not only the N-doping level but also the formation of the polymorphic phase. Structural and microstructural refinement obtained by XRD spectra and data processing performed by the Rietveld refinement revealed that TiO_2 obtained with HNO_3 present ca. 98 % of anatase and ca. 2% for rutile. Meanwhile TiO_2 nanoparticles synthesized with NH_4F and NH_4Cl present a single anatase phase with ca. 7.0 % and 4.4 % of Nitrogen substitutional Oxygen sites, respectively. The local structure of N-doped TiO_2 around Ti atoms was investigated by X-ray absorption spectroscopy. The XANES spectra show that N-doped TiO_2 possesses a characteristic pre-edge of single anatase structure. The coordination number decreased and the shrinking Ti-O bond distances are due to the N-doping in the TiO_2 structure. The most efficient Dye Sensitized solar cell and the higher hydrogen production was obtained from the TiO_2/NH_4Cl, which was obtained as single anatase phase with intermediary concentration o N substitutional oxygen sites.

Introduction

Within the last two decades many research groups have devoted their efforts to the development of efficient and clean ways to produce and store clean energy.[1–7] Solar Cells and hydrogen production by water splitting, comes to light as very promising alternatives to efficiently contribute to the world energetic matrix. In 1972, Fujishima and Honda presented to the world the possibility hydrogen production by water splitting[7] and in the last 40 years numerous researches have been conducted in order to boost the hydrogen generation efficiency and reduce the external applied potential.

About 25 years has passed since the work reported by O'Regan and Grätzel in 1991,[8] in this mean time many research groups have focused their efforts to the study of new electrolytes,[9–11] sensitizers[12–14] and semiconductors,[2,15] resulting in efficiencies of ca. 12%.[12] All this effort has made dye sensitized solar cells (DSSC) a promising candidate to efficiently contribute to the world energy matrix. In DSSC, in order to generate high photocurrent, upon photoexcitation the charge transfer from the highest occupied molecular orbital (LUMO) of the dye to the conduction band of TiO_2 must be faster than charge recombination between the photoexcited electron and the hole in the dye. Also the reduction of the oxidized lowest unoccupied molecular orbital (HOMO) by redox species in the electrolyte must be faster than the charge recombination reaction between the oxidized dye and injected photoexcited electrons in the semiconductor. Although different materials such as p-NiO, p-$CuInSe_2$, ZnO and SnO_2 have been studied, until now, TiO_2 photoanodes have resulted in the most efficient devices, allowing the fastest charge transfer rates.[16–19] In fact, due to the wide range of application, TiO_2 is the most extensively studied metal oxide. In order to obtain TiO_2 nanostructures presenting ideal properties for different applications, many works have been conducted on the effect of dopants, structural defects, sample preparation and thermal treatment on the TiO_2 properties. The results have shown that TiO_2 properties are directly related to the crystalline phase, crystal size, chemical structure and doping level.[20–24] For both photocatalytic hydrogen production and DSSC application, the anatase phase results in more efficient systems,[25–27] due to improved catalytic activity and electron mobility; therefore the control of phase formation during the synthesis and the solid-solid phase transformation during thermal treatment is a concern. A major drawback is the wide band gap of TiO_2, presenting absorption mostly only within the ultraviolet range. In order to overcome this issue,

[a] Instituto de Química, Universidade Federal do Rio Grande do Sul, 91501-970, Porto Alegre, RS, Brazil
[b] Instituto de Física, Universidade Federal do Rio Grande do Sul, 91501-970, Porto Alegre, RS, Brazil
[c] Instituto de Física de São Carlos, Universidade de São Paulo, CP 369, São Carlos 13560–970, SP, Brazil
[d] School of Chemistry, University of Nottingham, University Park, Nottingham, NG7 2RD, United Kingdom
Corresponding author: Tel .; + 55 51 3308 9625; + 55 51 3308 9626
e-mail address: mjls@ufrgs.br

band gap narrowing has been obtained by doping TiO_2 with metals such as Cu, Co, Ni, Mo, Fe, Ru, Au and Ag.[21,28–30] Although resulting in a wider absorption spectrum, studies have shown that metal impurities result in thermal instability. Another approach been explored is the doping by non-metallic elements.[22,31–33] Among the studied elements, nitrogen has been widely explored and many reports have shown different ways to dope TiO_2 with nitrogen and the effects on photocatalytic properties resulting in materials presenting high thermal stability, low carrier-recombination rates and higher ability to absorb light in the visible range.[34–39]

Although many works have been published on this subject, a wide experimental study on the effects of different nitrogen sources on the structural and microstructural properties of TiO_2, therefore on its optical and electronic properties is warranted to contribute to the a better control of this material. Herein, we synthesized N-doped TiO_2 nanoparticles obtained using three different nitrogen sources, HNO_3, NH_4Cl and NH_4F. The materials were characterized in detail by UV-Vis spectroscopy, XRD, Rietveld refinement, XANES, EXFAS and have been applied to assemble dye sensitized solar cells and to produce hydrogen by photolysis.

Experimental part

Synthesis of N-doped TiO_2 nanoparticles. Three samples of TiO_2 nanoparticles were obtained: i) through a well-known synthetic route using HNO_3 labelled as TiO_2/HNO_3,[40] ii) using NH_4F labelled as TiO_2/NH_4F and iii) using NH_4Cl labelled as TiO_2/NH_4Cl. The synthetic approach used to obtain TiO_2/NH_4F and TiO_2/NH_4Cl is also based on Grätzel work where 0.05M of acetic acid was added to 0.05M of titanium isopropoxide at room temperature. The solution was stirred for 15 min and poured into 72.5 mL of deionized water. The mixture was maintained under constant stirring for one hour at room temperature, to complete the hydrolysis. 0.025M of nitric acid 63% (NH_4F or NH_4Cl) was added. The mixture was stirred for 8 h at 80 ºC. After adding 95 mL of distilled water the solution was kept in autoclave and heated at 230 ºC for 12 h. Finally, all samples were rinsed with anhydrous ethanol, to remove residual H+ and water.

Microscopy Analysis. The morphology of the synthesized TiO_2 nanoparticles was obtained by Transmission Electron Microscopy (TEM) performed using a Libra Zeiss 120. For TEM, a small amount of sample was dispersed in isopropyl alcohol using a 450 W ultrasound horn and then depositing them onto a carbon-coated copper grid.

Absorption Spectra. Diffuse reflectance was performed using a Shimadzu UV-2450PC spectrophotometer with integrating sphere ISR-2200, at room temperature.

Specific Surface Area. N2 adsorption–desorption isotherms were determined at liquid nitrogen boiling point, using a micrometrics TriStar II equipped with krypton accessory. The samples were previously degassed at 140 °C under vacuum, during 6 hours. The specific surface areas were determined by BET multipoint method.

X-ray photoelectron spectroscopy. XPS experiments were carried out at beamline SXS of the Brazilian Synchrotron Light Laboratory. The operating pressure in the ultrahigh vacuum chamber (UHV) during the analysis was 1×10^{-9} Pa. The XPS spectra were collected using incident photon energy of 1840 eV. Energy steps were of 20 eV with 0.1 eV step energy and 200 ms per point acquisition time. The component of the C 1s peak of adventitious carbon was fixed at 285 eV to set the binding energy scale.

Crystalline Structure. X-ray powder diffraction (XRD) patterns were obtained using a Siemens D5000 diffractometer with Cu-Kα (λ= 1.5418 Å) in a 2θ range from 10 to 90° with a step size of 0.05° and time of 1 s per step. Rietveld refinements of the structure were carried out for all samples. The structural refinements were performed from X-ray diffraction patterns for the scale factor, atomic positions, anisotropic temperature factors and patterns parameters (peak widths, cell dimensions, zero point, background point interpolation, etc.) were also varied. The instrumental resolution function of the diffractometer was obtained from well-crystallized standard LaB_6 and taken into account in separated input files. Rietveld refinements were performed using the atomic position set and the space group of the Anatase structure $I4_1/amd$ N° 141. The unit cell is defined by the lattice vectors *a* and *c* and contains two TiO_2 units with Ti ions at *4b* Wyckoff positions (0,1/4,3/8), (0,3/4,5/8) and O ions at *8e* Wyckoff positions (0,1/4,***u***), (0,3/4,1/4+***u***), (1/2,1/4,-***u***+1/2) and (1/2,3/4,1/4-***u***) and Rutile structure $P4_2/mnm$, N° 136 the unit cell is defined by the lattice vectors *a* and *c* and contains two TiO_2 unit with Ti ions at *2a* Wyckoff positions (0,0,0), (½,½,½) and O ions at ***4f*** Wyckoff positions ±(***u***,***u***,0) and ±(***u***+½,½-***u***,½). The unit-cell parameters have been determined using x-ray diffraction and Rietveld refinement by means of the s software FullProf. The pseudo-Voigt profile function of Thompson, Cox and Hastings[41,42] was used with asymmetry correction at low angle. Corrections to the preferred orientation were performed using the Modified March's function. The anisotropic size broadening effects, related to the coherence volume of diffraction, were simulated using a model of spherical harmonics. [41,43,44]

Electron distribution density. The electron density on a point (x; y; z) of the crystallite cell with volume V was calculated by Fourier series using the structural factors F (hkl) obtained from Rietveld refinement.[45]

X-ray absorption spectroscopy (XAS) and data analysis. XAS spectra were measured on the K-edges of titanium (4966 eV) in transmission mode at room temperature using a channel-cut Si (111) crystal and three ionization chambers in the Brazilian Synchrotron Light Laboratory (LNLS, Campinas, Brazil) at the XAFS1 beamline. To calibrate the measurements, a Ti foil was used as reference sample. The powder samples were diluted with boron nitride and mounted on a tape. X-ray absorption near edge structure (XANES) data was measured from 80 eV below to 100 eV above the main absorption edge with energy step of 0.4 eV around the edge with 2s of acquisition per step. XAS data were analysed in accordance with the standard procedure for data reduction, using

ATHENA and ARTEMIS code from the IFEFFIT software package.[46] The EXAFS signal χ(k) was extracted and Fourier transformed (FT) using a Kaiser–Bessel window with a k-range from 2.2 to 11.2 Å−1.

Dye-sensitized Solar Cells Assembly. The TiO_2 pastes was screenprinted on the transparent conductive substrate (fluorine-doped tin oxide – FTO) previously soaked in 40 mM $TiCl_4$ aqueous solution at 60 °C for 30 minutes. The substrate was heated on a hot plate at 125 °C for 20 min and at 450°C for 30 min in a tubular oven. The mesoporous TiO_2 electrode was immersed in 0.5 mM cis-bis (isothiocyanato) bis (2,2'-bipyridyl-4,4'-dicarboxylato)-ruthenium(II)N-719 solution of acetonitrile/tertbutyl alcohol (1:1 v/v) and kept at room temperature 24 h. The counter-electrodes were prepared by coating the FTO surface with a 30 µL of 1 mM hexachloroplatinic acid and heated at 500°C. The mediator, responsible for the regeneration of the dye was placed in between the dye sensitized photoanode and the counter-electrode. The device was sealed using a polymeric film of low melting temperature (Meltonix). The electrolyte was a 0.6 M BMII, 0.03 M I_2, 0.10 M guanidinium thiocyanate and 0.5 M 4-tertbutylpyridine in a mixture of acetonitrile and valeronitrile.

Impedance spectra of DSSCs. Impedance spectra of DSSCs were recorded at open circuit potential, under 100 mW cm^{-2} bias illumination over a frequency range of 100 kHz – 10 mHz at signal amplitude of 10 mV using Autolab, PGSTAT100. Circuit fitting was complied by NOVA software.

Characterization of the Solar Cells. The performance of the DSSCs was evaluated by current versus potential measurements, carried out using a 300 W Xenon arc lamp and an AM1.5 filter. The power of the simulated light was calibrated to 100 mW/cm^2 and recorded by a picoamperimeter Keithley, model 2400.

Hydrogen production by photolysis. 10 mg of the photocatalyst: TiO_2/HNO_3, TiO_2/NH_4F or TiO_2/NH_4Cl was dispersed in a mixture of 7.5 mL of water and 2.5 mL of ethanol, kept in ultrasonic bath during 20 minutes and purged in argon. The samples were irradiated in a quartz cell by using a 240 W Xe lamp. The temperature was maintained constant at 25 °C using a cooling system. Hydrogen evolution was analysed with a gas chromatograph shimadzu 2014 equipped with a molecular column Siever 5 in a TCD detector using argon career. 50 µL aliquots were collected every 30 minutes and analysed.

Results and Discussion

The size and morphology of the TiO_2 NPs were investigated by TEM. **Fig.** 1 shows the images of the nanoparticles as synthesized (before thermal treatment). One can observe that all samples present the same shape and nearly the same size and size distribution of around 20 nm in diameter. Hence, the morphological properties are found not dependent on the source of nitrogen used during the synthesis.

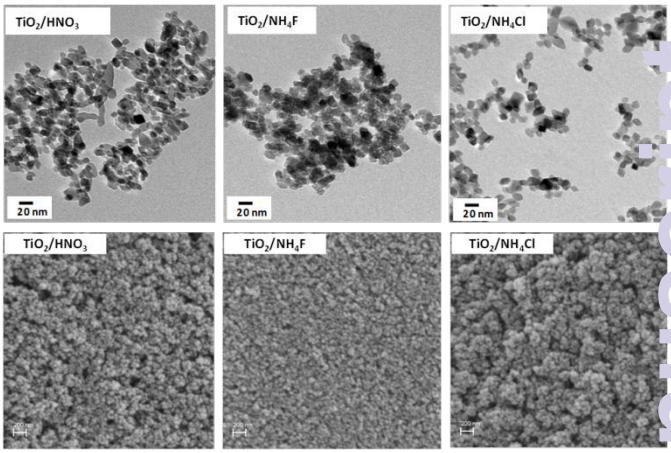

Fig. 1. (top) TEM images of the N-doped TiO_2 NPs prepared using different sources of nitrogen. (bottom) SEM images of the mesoporous films after thermal treatment at 500 °C.

The samples present similar energy band gaps with absorption edge at ca. 400 nm, towards the ultraviolet range (**Fig.** 2). The inset shows that nanoparticles obtained using NH_4Cl and NH_4F present a weak absorption band from ca. 400 to ca. 500 nm. Nitrogen have unpaired electrons which can easily bind to Ti4+ through acid-base reaction.[36,37] The absorption band observed from ca. 400 to ca. 500 nm is related to the interaction of mixed wave functions of nitrogen 2p with O 2p states, resulting in intermediary energy levels slightly above the top of the O 2p valence band of TiO_2.[38–40] Once the cations NH_4^+ are hydrolyzed to NH_3 and H_3O^+, the NH_3 seems to result in a slight higher doping level than NO_3^-. By considering the motion of NH_3 and NO_3^- within TiO_2; NH_3 has lager mobility once NO_3^- undergoes electrostatic interaction with the TiO_2 lattice. The expected larger diffusion of NH_3 would result in a larger degree of doping, after thermal treatment. Studies on bulk diffusion of N doped TiO_2 by NH_3 at high temperatures have suggested the presence of substitutional and interstitial nitrogen.[38,47] In addition, EPR studies has shown that calcination of NO^{3-} results in NO_2 species, meanwhile calcination of NH_3 results in NO.[48] Smaller molecules shall diffuse easily through the TiO_2 nanoparticles. The SEM images show that after thermal treatment, size and size distribution of the nanoparticles were maintained in the mesoporous film; however TiO_2/NH_4F seems to result in a more homogenous film.

Considering the formation of intermediary energy levels upon doping, a redshift of the absorption edge is expected along with an increase in doping. In this work the redshift was only observed for TiO_2/NH_4F, which also presented a slight more intense absorption band from 400 to 500 nm than TiO_2/NH_4Cl. Previous reports have shown that improved photocatalytic activity have been obtained by co-doping TiO_2 with both Nitrogen and Fluorine. The improved activity was attributed to a synergetic effect of the co-doping where fluorine atoms improved visible-light absorption.[49,50] Based on these previous results, for TiO_2/NH_4F, we should account for the presence of Fluorine atoms, however for refining the XRD data (discussed in next section) a good fitting was obtained by considering only nitrogen substitutional.

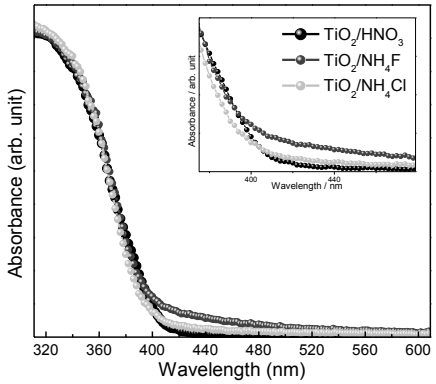

Fig. 2. Absorption spectra of N-doped TiO2 NPs synthesized using different sources of nitrogen, after thermal treatment at 500°C.

Fig. 3 shows the nitrogen adsorption-desorption isotherms of TiO_2/HNO_3, TiO_2/NH_4F and TiO_2/NH_4Cl as-synthesized and after thermal treatment at 500 °C. All samples show adsorption isotherms with a hysteresis type IV, characteristic of mesoporous material. The samples also present a small contribution of isotherms of the type I, characteristic of micropores. All of the isotherms present low nitrogen adsorption at P/P0 smaller than 0.4 values, and high nitrogen volume adsorption at high values of P/P0, above 0.8. After calcination the most significant change was observed from TiO_2/NH_4F, where a higher decrease on amount of nitrogen desorption, results from a decrease in surface area.[51,52]

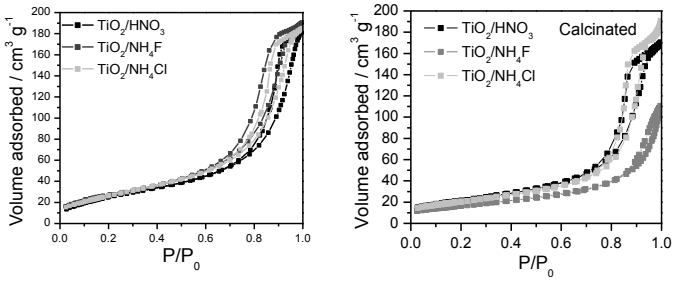

Fig. 3. N2 adsorption–desorption isotherms of the N-doped TiO_2 NPs prepared using different sources of nitrogen. (left) as-synthesized and (right) thermally treated at 500 °C.

Figure 4 shows the N 1s XPS spectra of TiO_2/HNO_3, TiO_2 /NH_4F and TiO_2 /NH_4Cl. One can observe a broad N 1s peak with maximum at 400 eV is observed in the spectra of N-doped samples. These values fit well with the binding energy for N-doped TiO_2 reported in the literature. Xiabo et al showed that the binding energy peak of N 1s, related to N-doped TiO_2 is a broad peak ranging from 397.4 eV to 403.7 eV. The discussion on interstitial and substitutional doping is rather difficult and the XPS assignment for interstitial or substitutional sites in N-doped TiO_2 has been the subject of a constant debate; as stated by Asahi et al, it is subject of controversial hypothesis.[54] XPS peaks within 399-400 eV have been attributed to Ti-O-N and Ti-N-O[55-57], to NH_3 adsorbed on the TiO_2 surface[57-59] and to either interstitial or substitutional nitrogen.[60-64] By refining the XRD data, the best fitting was obtained by considering substitutional nitrogen. For the sake of comparison, we have used the best possible fitting with statistically improved agreement factors, to evaluate the presence of Nitrogen in the TiO lattice. Therefore from the XPS and the XRD analyses it is reasonable to suggest that interstitial sites are preferentially formed at the surface while in the bulk substitutional nitrogen is observed, albeit very small

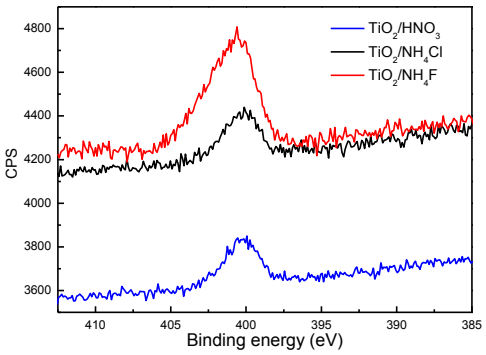

Fig. 4. N1S XPS spectra of TiO_2/HNO_3, TiO_2/NH_4F and TiO_2/NH_4Cl.

For the sake of comparison, we have used the best possible fitting with statistically improved agreement factors, to evaluate the presence of Nitrogen in the TiO_2 lattice. Therefore from the XPS and the XRD analyses it is reasonable to suggest that interstitial sites are preferentially formed at the surface while in the bulk substitutional nitrogen is observed, albeit very small.

Fig. 5 shows the XRD patterns and Rietveld refinement fitting results for all samples. TiO_2/HNO_3 presents diffraction peaks corresponding to the anatase phase (JCPDS# 84-1286) and small additional peaks related to the rutile phase (JCPDS # 76-0649). The percentages of anatase and rutile phases from TiO_2/HNO_3 were 98.21 ± 0.70 and 1.97% ± 0.01, respectively. In both anatase and rutile structures of TiO_2, each Ti_4^+ is surrounded by six species O_2^- resulting in an octahedral structure. The difference between the two polymorphic phases is related to different orthorhombic distortions of each octahedron and by the assembling of the octahedral resulting in the crystalline structure. For TiO_2/HNO_3 structural and microstructural refinement revealed that the phase of anatase was a tetragonal structure with an $I4_1/amd$ space group, with lattice parameters: a=b=3.7856 Å, c=9.5068 Å, α=β=γ= 90°, an average grain size of 16.40 ± 1.53 nm and micro-strain of 15.22 ± 0.0039 (%, 10^{-4}). In addition, the secondary phase associated to rutile was found a tetragonal structure with a $P4_2/mnm$ space group, with lattice parameters: a=b=4.5982 Å, c=2.9579 Å, α=β=γ= 90°, an average grain size of 48.82 ± 0.08 nm and a micro-strain (%, 10^{-4}) of 5.61 ± 0.0031. This difference in microstrain from anatase to rutile is mainly related to the dimension of the crystals.

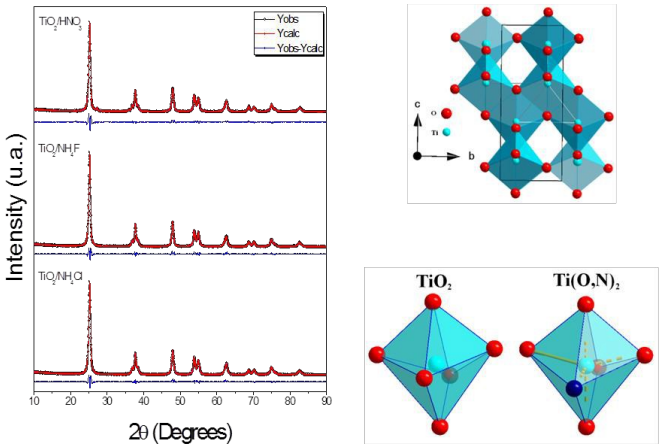

Fig. 5. XRD patterns and Rietveld refinement of TiO_2/HNO_3, TiO_2/NH_4F and TiO_2/NH_4Cl. Structures of the anatase phase of TiO_2.

As observed by XPS, TiO_2/ HNO_3 is also doped by Nitrogen. In fact, using the approach we have used to synthesize TiO_2, nitrogen doping is process intrinsic to the synthesis. We considered TiO_2/HNO_3 as a standard sample to compare how other nitrogen sources would affect the structure and the optical properties of the materials. For N-doped TiO2 the refinement proceeded by allowing a simultaneous presence of N and O at the 8e Wyckoff position. The atomic coordinates of N atoms were constrained to be the same as that of O. In order to study the influence of nitrogen incorporation on the sites of oxygen, the occupancies factors were let to vary freely. On the basis of chemical analysis, the rest of the positions were fixed to the theoretical occupancies factors. The occupancy factors are normalized in such a way as to represent the number of atoms in a formula unit.

Previous reports have shown that pH has a strong influence on the anatase and rutile phase formation in TiO_2.[65-68] In very acidic media the rutile phase have been found favoured over the anatase, meanwhile at intermediary pHs a single anatase phase can be obtained. Considering the previous studies suggesting that phase transformation from anatase to rutile is more difficult as the pH increases, a smaller concentration of H^+ resulting from the hydrolysis of NH_4^+ when compared to H^+ from HNO_3 is probably favoring the single anatase phase formation in TiO_2/NH_4F and TiO_2/NH_4Cl. In addition, in the conditions studied in this work we have observed that the presence both F^- and Cl^- either favours the formation of anatase phase or do not contribute significantly against it. This result is interesting once previous work in the literature shows that F^- and SO_4^{2-} contributes to the formation of anatase, while Cl^- favours the formation of the rutile phase.[69] Considering the anatase phase of TiO_2/NH_4F a tetragonal structure was found with an *I4₁/amd* space group, lattice parameters: a=b=3.7889 Å, c=9.5042 Å, α=β=γ= 90°, and an average grain size of 18.21 ± 2.44 nm and a micro-strain (%, 10^{-4}) of 18.50 ± 0.0078. In addition, by considering the TiO_2 sample a defect free lattice, a 2.9 % of Ti vacancy and a substitution of N in sites of O correspondents to 7.03%, were calculated for TiO_2/NH_4F. For the TiO_2/NH_4Cl a tetragonal structure was found with an *I4₁/amd* space group, lattice parameters: a=b=3.7858 Å, c=9.5059 Å, α=β=γ= 90°, and an average grain size of 14.19 ± 0.98 nm and a micro-strain (%, 10^{-4}) of 10.38 ± 0.0039. In addition a 0.14% of Ti vacancies and 4.43% of nitrogen substitutions in the oxygen sites were calculated. This result corroborates the absorption spectra (Fig. 2) showing that TiO_2/NH_4F presents a slight higher doping level than TiO_2/NH_4Cl and TiO_2/HNO_3. The average size for all of the samples and the shape of the grains were calculated using the modified Scherrer equation, using a model of spherical harmonics.[41,43]

$$\beta_h = \frac{\lambda}{D_h \cos\theta} = \frac{\lambda}{\cos\theta} \sum_{lmp} a_{lmp}\, y_{lmp}(\theta_h, \Phi_h)$$

Fig. 5 shows the shape of the crystallites calculated by Rietveld refinement using the XRD diffraction patterns. The image of the grains were projected on the x, y and z directions. The grains present the same growth feature on the x/y plane, however a different anisotropic growth is observed on the y/z and x/y planes. In addition a more spherical shape is expected for TiO_2/NH_4Cl.

These results are very interesting, once **Fig.** 2 shows that TiO_2/NH_4F presents a larger concentration of defects and that TiO_2/HNO_3 and TiO_2/NH_4Cl presents similar optical spectra. Therefore by considering the results observed in **Fig.** 6 we suggest relation between shape and concentration defects, where a more regular structure presents smaller defects concentration. The good agreement between the structure factors from the experimental data simulated by Rietveld Refinement, allowed us to obtain a Fourier electron density map, showing a two-dimensional mapping of the atoms inserted in the unit cell (**Fig.** 7).

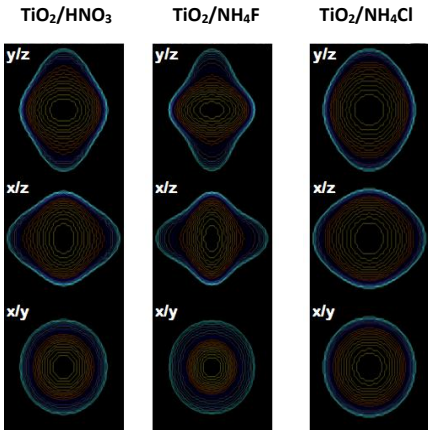

Fig. 6. Projected images of the crystallites shape calculated by Rietveld refinement using the XRD diffraction data.

Small changes in the surroundings of the sites related to oxygen and nitrogen substitutional are observed. When compared to the TiO_2/HNO_3 the TiO_2/NH_4F and the TiO_2/NH_4Cl present larger content of substitutional nitrogen. For TiO_2/NH_4F one can observe an electronic density reduction associated to the presence of substitutional nitrogen in the TiO_2 lattice. Similar behaviour is observed for TiO_2/NH_4Cl. Additionally, as earlier observed in **Fig.** 6, TiO_2 and TiO_2/NH_4Cl present similar electron density map meanwhile TiO_2/NH_4F presents a distinct behaviour probably related to the presence of the Fluorine ion.

In the anatase phase the Ti-Ti distances are larger than in the rutile, on the other hand the Ti-O distances are shorter. In the rutile phase each octahedron is surrounded by 10 neighbour

octahedrons, meanwhile in anatase each octahedron is surrounded by eight neighbours. This difference in structure can result in different mass densities and electronic band structures. In order to study the local structure around Ti atoms, we have carried out the XAS experiments at Ti K-edge.

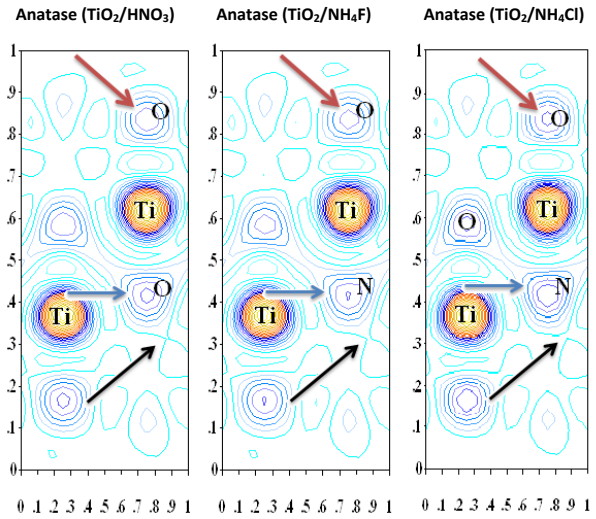

Fig. 7. Fourier electron density map for TiO_2/ HNO_3, TiO_2/NH_4/F and TiO_2/NH_4Cl.

The Ti K-edge XANES spectra for TiO_2/HNO_3, TiO_2/NH_4Cl and TiO_2/NH_4F is displayed in **Fig.** 8. The XANES pre-edge region was used to identify the local Ti coordination of the samples. All spectra have a very similar overall shape in the pre-edge and post edge regions. The pre-edge region of the samples shows a sharp peak that can be attributed to 1s to 3d transitions and the three pre-peaks in the same energy position in 4968.9, 4971.7 and 4974.1 eV that originates from the first and second coordination shells of Ti neighbours that gives evidence of the majority presence of TiO2 anatase-type structure.[59] The post-edge XANES spectra (region II) are similar to each other. However, the TiO_2/HNO_3 present slight changes in the spectral range from 4990 to 4995 eV (see arrows in **Fig 8**), with peaks features indicating the presence of the rutile phase. Therefore, TiO_2/HNO_3 present a mixture of majority TiO_2 anatase phase and small amount of rutile. Meanwhile the XANES spectra of TiO_2/NH_4Cl and TiO_2/NH_4F have the same single anatase crystalline structure, which corroborates the results obtained by XRD.[48]

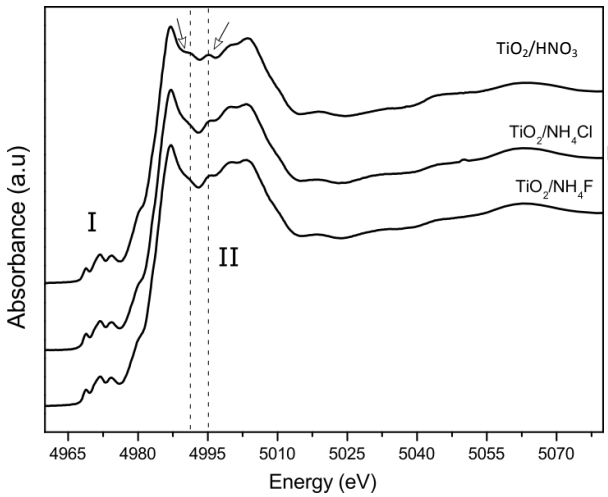

Fig.8. Ti K-edge XANES for TiO_2/HNO_3, TiO_2/NH_4Cl and TiO_2/NH_4F.

Fig. 9 (a, c, e) and (b, d, f) shows k3-weighted Ti K-edge EXAFS spectra and the corresponding Fourier Transforms (FT), respectively, for TiO_2/HNO_3, TiO_2/NH_4Cl and TiO_2/NH_4F. The k3-weighted EXAFS spectra of TiO_2/NH_4Cl and TiO_2/NH_4F (**Figs** 9 c, d) are very similar to each other, but different from the standard TiO_2 (**Fig.** 9a), that exhibit broad peak around at 4.5Å-1. This result indicates that the local environment around Ti atoms in TiO_2/NH_4Cl and TiO_2/NH_4F seems to resemble that in anatase crystalline structure, corroborating the previous discussion.

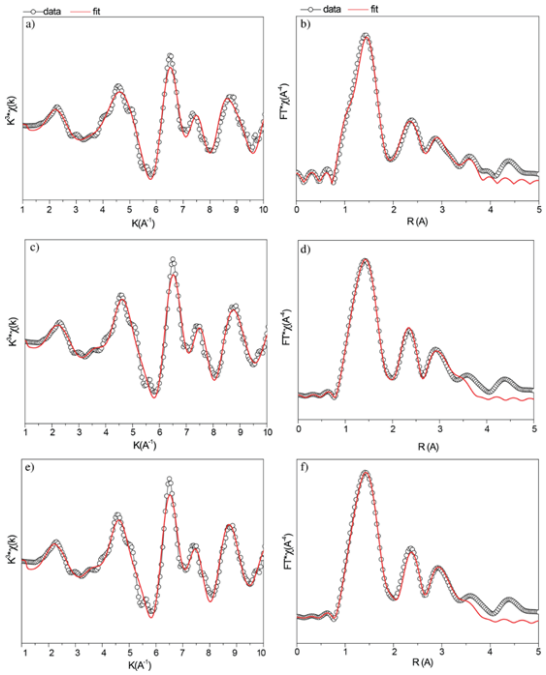

Fig. 9. (a, c, e) k3-weighted Ti K edge EXAFS signal and (b, d, f) the corresponding Fourier transform magnitude. Red lines represent the best fits obtained.

Fig. 9 (b, d and f) displays Ti K-edge FTs of EXAFS spectra corresponding to the shells of the Ti-O, Ti-Ti and O-Ti-O scattering path for the TiO_2. It can be seen that the FT features of all samples are look quite similar. The fitting results are summarized in Table 1. The best fitting results of the EXAFS spectra showed that the first peak at 1.96, 1.93 and 1.93 Å for TiO_2/HNO_3, TiO_2/NH_4Cl and

TiO_2/NH_4F, respectively, are due to the single-scattering path from first coordination shells of Ti-O bond by oxygen octahedron nearest neighbors around the Ti atom. Both N-doped TiO_2 NPs have Ti-O bond distances less than TiO_2/HNO_3 material. Table 1 show that all coordination numbers (N) for single Ti-O first shells are near to 6 that are close with theoretical value. Considering the uncertainties of EXAFS fittings, the N-doped TiO_2 samples prepared in NH4F and NH_4Cl possess the same coordination number. The smaller bond distances of the nearest Ti-O with respect to the TiO_2/HNO_3 sample suggests the presence of nitrogen doping in the structure of TiO_2 NPs.[69] The peaks appearing at 3.05, 3.04 and 3.04 Å are due to Ti-Ti bond distances at second shell. The shrinking Ti-Ti second shell coordination and increasing of Debye-Waller factor is an indication of increasing in disorder in TiO_2 structure probably due to the N doping.

Table 1. EXAFS fitting parameters: $_a$coordination numbers (N), $_b$bond length (Å) and $_c$Debye-Waller factor (σ2) for N-doped TiO_2 samples

Sample	scattering	^{a}R (Å)	^{b}N	$^c\sigma^2(10^{-3}Å^2)$
TiO_2/HNO_3	Ti-O	1.96 ±0.02	6.39 ± 0.16	6.30 ± 0.01
	Ti-Ti	3.05 ±0.01	3.30 ± 0.10	4.80 ± 0.02
TiO_2/NH_4Cl	Ti-O	1.93 ±0.062	5.70± 0.74	4.80 ± 0.01
	Ti-Ti	3.04 ±0.076	3.74 ± 0.85	5.10 ± 0.02
TiO_2/NH_4F	Ti-O	1.93 ± 0.004	5.85 ± 0.76	5.10 ± 0.16
	Ti-Ti	3.04 ± 0.010	3.98 ± 0.92	6.40± 0.24

From the current versus potential curves (**Fig.** 10), we have obtained the short-circuit current (Isc), open circuit voltage (Voc), Fill Factor (FF) and efficiency (η) from the devices assembled with the three TiO_2 samples (Table 2). The device assembled with TiO_2/NH_4Cl presents improved FF. Considering the data obtained from XRD, Rietveld refinement, XANES and EXAFS we can relate this result to the presence of a single phase anatase and to a lower concentration of detects (0.14% of Ti vacancies in and 4.43% of nitrogen substitutions in the oxygen sites). These properties result in improved electron mobility by hoping from one nanoparticle to another, in order to reach the charge collecting electrode.

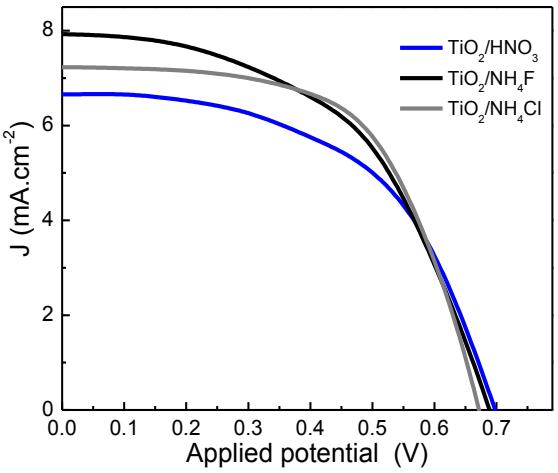

Fig. 10. Current *versus* potential curves from the devices assembled with TiO_2/ HNO_3, TiO_2/NH_4F and TiO_2/NH_4Cl.

The electron transport through the TiO_2 network towards the collection electrode occurs by diffusion and is limited by trapping and detrapping from defects within the nanoparticles and at and across grain boundaries, hindering charge mobility. We suggest that the presence of rutile domains in the TiO_2 results in loss of electron mobility and therefore in loss of efficiency. In addition, the nitrogen doped mesoporous structures present lower charge recombination rate at the TiO_2/electrolyte interface.

Table 2. Electrical parameters and the efficiency of the assembled devices

	I_{sc} (mA)	V_{oc} (V)	*FF* (%)	η (%)
TiO_2/HNO_3	6.4	0.72	54	2.5
TiO_2/NH_4F	7.9	0.71	51	2.8
TiO_2/NH_4Cl	7.2	0.70	60	3.0

Fig. 11 shows the results obtained from hydrogen production performed by photolysis in ethanol/water solution. The lowest efficiency was obtained from TiO_2/HNO_3 presenting hydrogen production rate of 0.15 mmol.g-1h-1 while TiO_2/NH_4Cl present a two fold increase, resulting in hydrogen production rate of 0.3 mmol.g-1h-1. The literature shows many works where Nitrogen doped TiO_2 and bare TiO_2 present similar photocatalytic activity under UV light but improved photocatalytic activity under visible light is obtained by N-doped TiO_2.[72,73] Some works correlate the enhancement in photocatalytic activity on the intensity of the peak at 400–404 eV.[73,74]

These results corroborate the DSSC measurements, showing that the intermediary doping combined to the single anatase phase, which results in higher photocurrent and lower recombination rate favours both photolysis and solar cell efficiency.

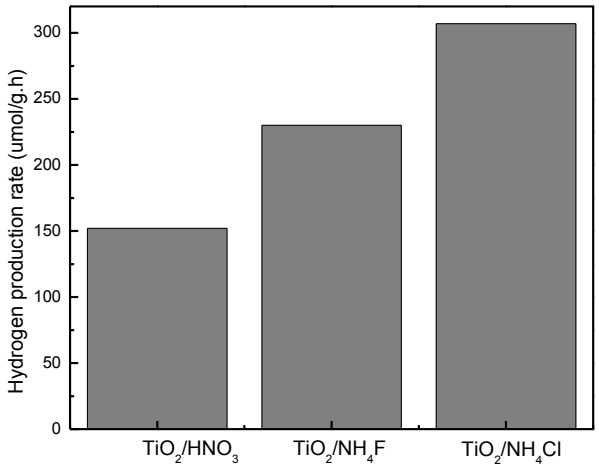

Fig. 11. Graph showing hydrogen production from TiO_2/ HNO_3, TiO_2/NH_4F and TiO_2/NH_4Cl.

Fig. 12 compares the Nyquist plots of the assembled DSSCs. These plots consist of three components; ohmic resistance R_0, the left arcs (R_1) (observed in the high frequency region > 1 kHz) and the larger arcs (R_2) (observed in the frequency range of 100– 50 Hz). According to the literature,[75-77] the arcs in the high frequency represent the redox reaction at Pt/electrolyte interface while the arcs at lower frequency are attributed to the TiO_2/electrolyte interface. Table 3 summarizes the results obtained by fitting the experimental data, using an equivalent circuit containing a combination of constant phase element (CPE) and resistance components (inset of **Fig. 12);** where CPE_1 and CPE_2 correspond to R_1 and R_2, respectively.[78] These impedances have an obvious effect on the charge transportation in the DSSCs.

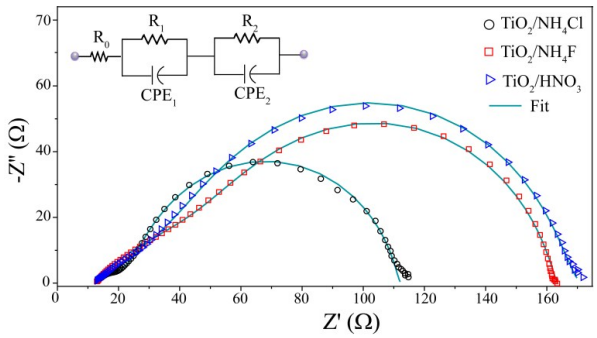

Fig. 12 Impedance spectra of the DSSCs from TiO_2/HNO_3, TiO_2/NH_4F and TiO_2/NH_4Cl. The inset gives the equivalent circuit used to fit the impedance data; where CPE_1 and CPE_2 are the constant phase elements.

Consequently, the cell performance is improved when the total resistance ($R_{total} = R_0 + R_1 + R_2$) is small.[75-77] One can observe that the R_{total} for TiO_2/NH_4Cl and TiO_2/NH_4F is smaller than for TiO_2/HNO_3. In addition, the smallest R_{total} is obtained from TiO_2/NH_4Cl, which should present improved charge transportation and higher photoelectrochemical performance. These results are consistent with the energy conversion efficiency presented in Table 2

Table 3. EIS Parameters of the Three Devices Determined by Fitting the Data According to the Equivalent Circuit Model (See Fig. 12).

sample	R_0 (Ω)	R_1 (Ω)	R_2(Ω)	R_{total}(Ω)
TiO_2/NH_4Cl	11.78	20.76	80.69	113.23
TiO_2/NH_4F	11.39	53.20	97.91	162.50
TiO_2/HNO_3	12.14	55.26	103.41	170.81

Conclusions

In this work we show that single anatase phase TiO_2 nanoparticles can be obtained by tuning the nitrogen source used during the synthesis. The use of NH_4^+ which is hydrolyzed to NH_3 leads to the formation of a single anatase phase, meanwhile NO_3^- was found to result in a mixed anatase/rutile lattice. In addition, we have observed a dependence of the amount of nitrogen on the source of nitrogen, hence effecting doping level and electronic properties of the nanoparticles. Although only a small change in the optical spectra was detected, the changes observed by XRD, XANES and EXAFS shows that the efficiency of Dye sensitized solar cells and hydrogen production are deeply dependent on the N-doping of the semiconductor.

Acknowledgements

The authors are grateful for financial support from the following Brazilian agencies: Conselho Nacional de Desenvolvimento Científico e Tecnológico (Processos 477804/2011-0, 490221/2012-2 and 472243/2013-6). Our thanks are also extended to the Brazilian Synchrotron Light Laboratory (LNLS) for use of its XAFS1 experimental facilities (proposal XAFS1- 17154).

Notes and references

1 N. Tétreault, M. Grätzel, Novel Nanostructures for next Generation Dye-Sensitized Solar Cells, Energy Environ. Sci. 2012, **5**, 8506.

2 M. T. Laranjo, N. C. Ricardi, L. T. Arenas, E. V. Benvenutti, M. C. de Oliveira, M. J. L. Santos, T. M. H. Costa, TiO_2 and TiO_2/SiO_2 Nanoparticles Obtained by Sol-Gel Method and Applied on Dye Sensitized Solar Cells. J. Sol-Gel Sci. Technol 2014, **72**, 273–281.

3 J. A. Fernandes, P. Migowski, Z. Fabrim, A. F. Feil, G. Rosa, S. Khan, G. J. Machado, P. F. P. Fichtner, S. R. Teixeira, M. J. L. Santos, TiO_2 Nanotubes Sensitized with CdSe via RF Magnetron Sputtering for Photoelectrochemical Applications under Visible Light Irradiation, Physical Chemistry Chemical Physics 2014, **16**, 9148–9153.

4 R. G. Sabat, M. J. L Santos.; P. Rochon, S Surface Plasmon-Induced Band Gap in the Photocurrent Response of Organic Solar Cells. Int J Photoenergy 2010, **2010**, ID 698718, 5.

5 Y. Shi, R. B. M. Hill, J. H. Yum; A. Dualeh, SBarlow, M. Grätzel, S. R. Marder, M. K. A Nazeeruddin, High-Efficiency Panchromatic Squaraine Sensitizer for Dye-Sensitized Solar Cells, Angew. Chemie - Int. Ed. 2011, **50**, 6619–6621.

6 X. Fan, Z. Chu, F. Wang, C. Zhang, L. Chen, Y. Tang, D. Zou, Wire-Shaped Flexible Dye-Sensitized Solar Cells. Adv. Mater. 2008, **20**, 592–595.

7 A. Fujishima, K. Honda, Nature 1972, **238**, 37-38.

8 B. O'Regan, M. Grätzel, A Low-Cost, High-Efficiency Solar Cell Based on Dye-Sensitized Colloidal TiO_2 Films. Nature, 1991, **353**, 737–740.

9 N. Papageorgiou, Y. Athanassov, M. Armand, P. Bonho te.; H. Pettersson, A. Azam; M. Grätzel The Performance and Stability of Ambient Temperature Molten Salts for Solar Cell Applications. J. Electrochem. Soc. 1996**,** **143**, 3099–3108.

10 U. Scherf, Counterion Pinning in Conjugated Polyelectrolytes for Applications in Organic Electronics. Angew. Chemie - Int. Ed. 2011, **50**, 5016–5017.

11 W. Zhang, J. Li, S. Jiang, Z.-S. Wang, POSS with Eight Imidazolium Iodide Arms for Efficient Solid-State Dye-Sensitized Solar Cells. Chem. Commun. (Camb). 2014, **50**, 1685–1687.

12 F. Gao, Y. Wang, D. Shi, J. Zhang, M. Wang, X. Jing, R.Humphry-baker, P. Wang, S. M. Zakeeruddin, M. Gra, Enhance the Optical Absorptivity of Nanocrystalline TiO Film with High Molar Extinction Coefficient Ruthenium Sensitizers for High Performance Dye-Sensitized Solar Cells Enhance the Optical Absorptivity of Nanocrystalline TiO_2 Film with High Molar Extinc. J. Am. Chem. Soc. 2008, **130**, 10720–10728.

13 C.-W. Lee, H.-P. Lu, C.-M. Lan, Y.-L. Huang, Y.-R. Liang, W.-N. Yen, Y.-C. Liu, Y.-S. Lin, E. W.-G. Diau, C.-Y. Yeh, Novel Zinc Porphyrin Sensitizers for Dye-Sensitized Solar Cells: Synthesis and Spectral, Electrochemical, and Photovoltaic Properties. Chemistry 2009, **15**, 1403–1412.

14 S. Ito, H. Miura, S. Uchida, M. Takata, K. Sumioka, P. Liska, P. Comte, P. Péchy, M. Grätzel, High-Conversion-Efficiency Organic Dye-Sensitized Solar Cells with a Novel Indoline Dye. Chem. Commun. (Camb). 2008, **41**, 5194–5196.

15 S. Ito, M. K. NazeeruddinP. S. M. ZakeeruddinP. , Péchy, P. Comte M. , Gratzel, T. Mizuno, A. Tanaka, T. Koyanagi, Study of Dye-Sensitized Solar Cells by Scanning Electron Micrograph Observation and Thickness Optimization of Porous TiO_2 electrodes. Int. J. Photoenergy 2009, **2009**, 12–14.

16 S. A. Haque, Y. Tachibana, D. R. Klug, J. R. Durrant, Charge Recombination Kinetics in Dye-Sensitized Nanocrystalline Titanium Dioxide Films under Externally Applied Bias. J. Phys. Chem. B 1998, **102**, 1745–1749.

17 S. Ardo, G. J. Meyer, Photodriven Heterogeneous Charge Transfer with Transition-Metal Compounds Anchored to TiO_2 Semiconductor Surfaces. Chem. Soc. Rev. 2009, **38**, 115–164.

18 Y. Tachibana, J.-E. Moser, M. Grätzel, D. R. Klug, J. R. Durrant, Subpicosecond Interfacial Charge Separation in Dye-Sensitized Nanocrystalline Titanium Dioxide Films. J. Phys. Chem. 1996, **100**, 20056–20062.

19 H. B. Storck, W Willig, F, T. B. Measurement of Ultrafast Photoinduced Electron Transfer from Chemically Anchored Ru-Dye Molecules into Empty Electronic States in a Colloidal Anatase TiO_2 Film. J. Phys. Chem. B 1997, **101**, 6802.

20 A. Di Paola, G. Marcì, L. Palmisano, M. Schiavello, K. Uosaki, S. Ikeda, B. Ohtani, Preparation of Polycrystalline TiO_2 Photocatalysts Impregnated with Various Transition Metal Ions: Characterization and Photocatalytic Activity for the Degradation of 4-Nitrophenol. J. Phys. Chem. B 2002, **106**, 637–645.

21 A. Fuerte, M. D. Hernández-Alonso, A. J. Maira, A. Martínez-Arias, M. Fernández-García; J. C. Conesa, J. Soria, Visible Light-Activated Nanosized Doped-TiO_2 Photocatalysts. Chem. Commun. 2001, **24**, 2718–2719.

22 S. Sato, R. Nakamura, S. Abe, Visible-Light Sensitization of TiO2 Photocatalysts by Wet-Method N Doping. Appl. Catal. A Gen. 2005, **284**, 131–137.

23 R. Asahi, T. Morikawa, T. Ohwaki, K. Aoki, Y. Taga, Visible-Light Photocatalysis in Nitrogen-Doped Titanium Oxides. Science. 2001, **293,** 2000–2002.

24 Y. Hwu, Y. D. Yao, N. F. Cheng, C. Y. Tung, H. M. Lin, X-Ray Absorption of Nanocrystal TiO2. Nanostructured Mater. 1997 **9**, 355–358.

25 J. Zhang, P. Zhou, J. Liu, J. Yu, New Understanding of the Difference of Photocatalytic Activity among Anatase, Rutile and Brookite TiO_2. Phys. Chem. Chem. Phys. 2014, **16**, 20382–20386.

26 Y. Wang, L. Li, X. Huang, Q. Li, G. Li, New Insights into Fluorinated TiO2 (brookite, Anatase and Rutile) Nanoparticles as Efficient Photocatalytic Redox Catalysts. RSC Adv. 2015, **5**, 34302–34313.

27 X. Wang, A. Kafizas, X. Li, S. J. A. Moniz, P. J. T. Reardon, J. Tang, I. P. Parkin, J. R. Durrant, Transient Absorption Spectroscopy of Anatase and Rutile: The Impact of Morphology and Phase on Photocatalytic Activity. J. Phys. Chem. C 2015, 150423173617003.

28 A. Di Paola, G. Cufalo, M. Addamo, M. Bellardita, R. Campostrini, M. Ischia, R. Ceccato, L. Palmisano, Photocatalytic Activity of Nanocrystalline TiO2 (brookite, Rutile and Brookite-Based) Powders Prepared by Thermohydrolysis of $TiCl_4$ in Aqueous Chloride Solutions. Colloids Surfaces A Physicochem. Eng. Asp. 2008, **317**, 366–376.

29 J. Zhu, F. Chen, J. Zhang, H. Chen, Anpo, M. Fe3+-TiO2 Photocatalysts Prepared by Combining Sol-Gel Method with Hydrothermal Treatment and Their Characterization. J. Photochem. Photobiol. A Chem. 2006, **180**, 196–204.

30 H. Yamashita, M. Harada, J. Misaka, M. Takeuchi, Y. Ichihashi, Goto, F.; M. Ishida, T. Sasaki, M. Anpo, Application of Ion Beam Techniques for Preparation of Metal Ion-Implanted TiO_2 Thin Film Photocatalyst Available under Visible Light Irradiation: Metal Ion-Implantation and Ionized Cluster Beam Method. J. Synchrotron Radiat. 2001, 8, 569–571.

31 Y. Cong, J. Zhang, F. Chen, M. Anpo, Synthesis and Characterization of Nitrogen-Doped TiO2 Nanophotocatalyst with High Visible Light Activity. J. Phys. Chem. C 2007, **111**, 6976–6982.

32 T. Ohno, T. Mitsui, M. Matsumura, Photocatalytic Activity of S-Doped TiO2 Photocatalyst under Visible Light. Chem. Lett. 2003, **32**, 364–365.

33 Y. Liu, X. Chen, J. Li, C. Burda, Photocatalytic Degradation of Azo Dyes by Nitrogen-Doped TiO2 Nanocatalysts. Chemosphere 2005, **61**, 11–18.

34 S. Rodrigues, K. T. Ranjit, S. Uma, I. N. Martyanov, K. J. Klabunde, Single-Step Synthesis of a Highly Active Visible-Light Photocatalyst for Oxidation of a Common Indoor Air Pollutant Acetaldehyde. Adv. Mater. 2005, **17**, 2467–2471.

35 I. Paramasivam, H. Jha, N. Liu, P. Schmuki, A Review of Photocatalysis Using Self-Organized TiO2 Nanotubes and Other Ordered Oxide Nanostructures. Small 2012, 8, 3073–3103.

36 R. P. Vitiello, J. M. Macak, A. Ghicov, H. Tsuchiya, L. F. P. Dick, P. Schmuki, N-Doping of Anodic TiO_2 Nanotubes Using Heat

Treatment in Ammonia. Electrochem. commun. 2006, **8**, 544–548.

37 R. Nakamura, T. Tanaka, Y. Nakato, Mechanism for Visible Light Responses in Anodic Photocurrents at N-Doped TiO2 Film Electrodes. J. Phys. Chem. B 2004, **10**8, 10617–10620.

38 O. Diwald, T. L. Thompson, T. Zubkov, S. D. Walck, J. T. Yates, Photochemical Activity of Nitrogen-Doped Rutile TiO2 (110) in Visible Light. J. Phys. Chem. B 2004, **108**, 6004–6008.

39 J. A Rodriguez, T. Jirsak, J. Dvorak, S. Sambasivan, D. Fischer, Reaction of NO2 with Zn and ZnO: Photoemission, XANES, and Density Functional Studies on the Formation of NO_3. J. Phys. Chem. B 2000, 104, 319–328.

40 S. Ito, T. N. Murakami, P. Comte, P. Liska, Grätzel, C.; Nazeeruddin, M. K.; Grätzel, M. Fabrication of Thin Film Dye Sensitized Solar Cells with Solar to Electric Power Conversion Efficiency over 10%. Thin Solid Films 2008, **516**, 4613–4619.

41 J. Rodríguez-Carvajal, Recent Advances in Magnetic Structure Determination by Neutron Powder Diffraction. Phys. B Condens. Matter 1993, **192**, 55–69.

42 P. Thompson, D. E. Cox, J. B. Hastings, Rietveld Refinement of Debye–Scherrer Synchrotron X-Ray Data from Al2O3. J. Appl. Crystallogr. 1987, **20**, 79–83.

43 W. A. Dollase, correction of intensities of preferred orientation powder diffractometry: Application of the March Model J. Appl. Crystallogr. 1986, 19, 267–272.

44 L. B. McCusker, R. B. Von Dreele, D. E. Cox, D. Louër, P. Scardi, Rietveld Refinement Guidelines. Journal of Applied Crystallography. 1999, 36–50.

45 J. K. Burdett, T. Hughbanks, G. J. Miller, J. W. Richardson, J. V. Smith, Structural-Electronic Relationships in Inorganic Solids: Powder Neutron Diffraction Studies of the Rutile and Anatase Polymorphs of Titanium Dioxide at 15 and 295 K. J. Am. Chem. Soc. 1987, **109**, 3639–3646.

46 B. Ravel; M. Newville, ATHENA, ARTEMIS, HEPHAESTUS: Data Analysis for X-Ray Absorption Spectroscopy Using IFEFFIT. In Journal of Synchrotron Radiation; 2005; **12,** 537–541.

47 R. G. Palgrave; D. J. Payne; R. G. Egdell, Nitrogen Diffusion in Doped TiO2 (110) Single Crystals: A Combined XPS and SIMS Study. J. Mater. Chem. 2009, **19,** 8418–8425.

48 C. Di Valentin; E. Finazzi; G. Pacchioni; A. Selloni; S. Livraghi; M. C. Paganini; E. Giamello, N-Doped TiO2: Theory and Experiment. Chem. Phys. 2007, **339**, 44–56.

49 C. Di Valentin, G. Pacchioni; Catalysis Today. **2013,** 206, 12–18

50 D. Huanga, S. Liao a, J. Liu, Z. Danga, L. Petrik; Journal of Photochemistry and Photobiology A: Chemistry. **2006,** 184, 282–288

51 J. C. Yu, J. Yu, W. Ho, Z. Jiang; L. Zhang, Effects of F-Doping on the Photocatalytic Activity and Microstructures of Nanocrystalline TiO2 Powders. Chem. Mater. 2002, **14**, 3808–3816.

52 L. Lo Presti, M. Ceotto, F. Spadavecchia, G. Cappelletti, D. Meroni, R. G. Acres, S. Ardizzone, Role of the Nitrogen Source in Determining Structure and Morphology of N-Doped Nanocrystalline TiO2. J. Phys. Chem. C 2014, **118**, 4797–4807.

53 Xiaobo Chen, Clemens Burda, J. Phys. Chem. B 2004, 108, 15446-15449

54 Ryoji Asahi, Takeshi Morikawa, Hiroshi Irie, Takeshi Ohwak Nitrogen-Doped Titanium Dioxide as Visible-Light-Sensitive Photocatalyst: Designs, Developments, and Prospects Chem. Rev. 2014, 114, 9824−9852

55 Jin Wang, De Nyago Tafen, James P. Lewis, Zhanglian Hong, Ayyakkannu Manivannan, Mingjia Zhi, Ming Li, Nianqiang Wu Origin of Photocatalytic Activity of Nitrogen-Doped TiO2 Nanobelts J. Am. Chem. Soc. 2009, 131 (39) 12290 – 12297.

56 Xu J H, Li J X, Dai W L, Cao Y, Li H X, Fan K N, Simple fabrication of twist-like helix N, S-codoped titania photocatalyst with visible-light response. Appl. Catal. B: Environ. 2008; 79: 72-80

57 M. Sathish, B. Viswanathan, R.P. Viswanath, C.S. Gopinath, Chem.Mater. 17 (2005) 6349

58 Moulder, J. F.; Stickle, W. F.; Sobol, P. E.; Bomben, K. D. Handbook of X-ray photoelectron Spectroscopy; Eden Prairie: 1992.

59 Jansen, R. J. J.; Van Bekkum, H. Carbon 1995, 33, 1021.

60 B. Viswanathan and K. R. Krishanmurthy, Nitrogen Incorporation in TiO2: Does It Make a Visible Light Photo-Active Material? International Journal of Photoenergy, Vol. 2012, article ID 269654.

61 J.Wang, D. N. Tafen, J. P. Lewis et al., "Origin of Photocatalytic Activity of Nitrogen-Doped TiO2 Nanobelts," *Journal of the American Chemical Society*, vol. 131, no. 341, pp. 229 12297, 2009.

62 Y. Cong, J. Zhang, F. Chen, M. Anpo, and D. He, "Preparation, photocatalytic activity, and mechanism of nano-TiO2 Codoped with nitrogen and iron (III)," *Journal of Physical Chemistry C*, vol. 111, no. 28, pp. 10618–10623, 2007

63 J. Yang, H. Bai, X. Tan, and J. Lian, "IR and XPS investigation of visible-light photocatalysis-Nitrogen-carbon-doped TiO2 film," *Applied Surface Science*, vol. 253, no. 4, pp. 1988–1994, 2006.

64 D. Mitorj and N. H. Kisch, "The nature of nitrogen-modified titanium dioxide photocatalysts active in visible light," *Angewandte Chemie International Edition*, vol. 47, no. 51, pp. 9975– 9978, 2008

65 R. Parra, M. S. Goes, M. S. Castro, E. Longos, P. R. Bueno, J. A Varela, "Reaction pathway to the synthesis of anatase via the chemical modification of titanium isopropoxide with acetic acid," *Chemistry of Materials*, 2008, **20**, 143–150.

66 X. Chen, G. Gu, "Study on synthesis of nanometer TiO_2 crystal from organic compound in liquid phase at normal pressure and low temperature", *Chin. J. Inorg. Chem*., 2002, 18(7), 749—752.

67 Y. Hu, H.-L. Tsai, C.-L. Huang, "Effect of brookite phase on the anatase-rutile transition in titania nanoparticles," *Journal of the European Ceramic Society*, 2003, **23**, 691–696;

68 S. M. Abdel-Azim, A. K. Aboul-Gheit, S. M. Ahmed, D. S. El-Desouki, M. S. A. Abdel-Mottaleb. "Preparation and Application of Mesoporous Nanotitania Photocatalysts Using Different Templates and pH Media" *International Journal of Photoenergy*, 2014, Article ID 687597, 1-11.

69 J. M. Wu, S. Hayakawa, K. Tsuru, A. Osaka, "Porous Titania Films Prepared from Interactions of Titanium with Hydrogen Peroxide Solution" Scr. Mater. 2002, **46**, 101–106.

70 T. Kubo, A. Nakahira, Local Structure of TiO2-Derived Nanotubes Prepared by the Hydrothermal Process. J. Phys. Chem. C 2008, **112**, 1658–1662.

71 C. Belver, R. Bellod, S. J. Stewart, F. G. Requejo, M. Fernández-García, Nitrogen-Containing TiO2 Photocatalysts. Part 2. Photocatalytic Behavior under Sunlight Excitation. Appl. Catal. B Environ. 2006, **65**, 309–314.

72 R. Asahi, T. Morikawa, T. Ohwaki, K. Aoki, Y. Taga, SCIENCE VOL 293 13 JULY 2001.

73 Yu, J. G.; Zhou, M. H.; Cheng, B.; Zhao, X. J. J. Mol. Catal. A: Chem. 2006, 246, 176.

74 X.B. Chen, C. Burda, J. Phys. Chem. B 108 (2004) 15446

76 T. Hoshikawa, T. Ikebe, R. Kikuchi, K. Eguchi, Effects of electrolyte in dye-sensitized solar cells and evaluation by impedance spectroscopy Electrochimica Acta 2006, **51**, 5286 – 5294

77 X. Sun, Y. Liu, Q. Tai, B. Chen, T. Peng, N. Huang, S. Xu, T. Peng, X.-Zhong Zhao, High Efficiency Dye-Sensitized Solar Cells based on a Bi-Layered Photoanode Made of TiO2 Nanocrystallites and Microspheres with High Thermal Stability *J. Phys. Chem. C*, 2012, ***116*** (22), 11859–11866

78 Q. Wang, J.-E. Moser, M. Gratzel, Electrochemical Impedance Spectroscopic Analysis of Dye-Sensitized Solar Cells, J. Phys. Chem. B 2005, **109**, 14945-14953.